Solvent Effects and Internal Functions Control Molecular Recognition of Neutral Substrates in Functionalized Self-Assembled Cages

Connor Z. Woods, Komal Sharma, Chengwei Chen, Lei Yang, Junyi Chen, Yu-Chen Wu, Naira S. Farooqi, Jingsong Zhang, Ryan R. Julian and Richard J. Hooley*

Department of Chemistry and the UCR Center for Catalysis, University of California-Riverside, Riverside, CA 92521, U.S.A.

Supporting Information Placeholder

ABSTRACT: A suite of internally functionalized Fe_4L_6 cage complexes has been synthesized with lipophilic endgroups to allow dissolution in varied solvent mixtures, and the scope of their molecular recognition of a series of neutral, non-polar guests analyzed. The lipophilic endgroups confer cage solubility in solvents with a wide range of polarities, from HFIP to THF, and the hosts show micromolar affinities for neutral guests, despite having no flat panels enclosing the cavity. These hosts allow interrogation of the effects of internal functional group on guest binding properties, as well as solvent-based driving forces for recognition. Introducing polar effects to the interior of the cavity enhances guest binding affinity in non-polar solvents, adding space-filling aliphatic groups reduces affinity in all cases. While high dielectric solvents such as acetonitrile strongly favor guest binding, "low dielectric, high polarity" solvents such as hexafluoroisopropanol strongly occupy the cavity and prevent guest recognition. Analysis of the cage optical transitions shows that the guests interact with the central ligand cores and reside in close proximity to the internal functions. These results have implications for supramolecular catalysis: balancing directed host:guest interactions (e.g. H-bonds) with entropic effects from solvent displacement is essential for reactions in these (and related) biomimetic hosts.

INTRODUCTION

Self-assembled metal-ligand cage complexes have multiple applications dependent on selective molecular recognition, including supramolecular catalysis.[1] Substrates can be cationic,[2] anionic[3] and/or neutral,[4] with differing behaviors in different solvents: binding neutral species can be favored in water via the hydrophobic effect, for example.[5] The most effective way to enable strong substrate binding in a self-assembled cage is to fully surround a guest with a defined cavity for occupancy. Cages formed from large flat ligands that display small entry portals maximize size-based binding selectivity, and confer slow guest exchange on the guests.[6] Slow exchange is beneficial for recognition, but less so for catalysis, where substrate turnover is paramount: cages with large entry portals allow rapid substrate entry and exit,[7] often at the cost of selectivity. Substrate binding selectivity can be enhanced by a judicious choice of solvent, and this is also vital for supramolecular catalysis. Different reaction types are favored in different solvents, for example Bronsted-acid catalyzed processed are favored in non-polar solvents.[8] Understanding the effects of solvent on the molecular recognition properties of catalytically active self-assembled cage hosts will enable a far greater scope of reactions to be accessed.

There are many beautiful examples of quantitating solvent effects on guest recognition, focusing on both directed interactions between host and guests, such as shape-filling, H-bonding, π-stacking and ion pairing,[7,9] or the effects of solvent expulsion from the cavity (most often in water).[5] Diederich's pioneering work analyzing solvent dependence on molecular recognition of neutral species in a "non-enclosed" receptor[10] showed that the binding affinities of pyrene in a neutral cyclophane macrocycle were dependent on the polarity of the solvent; more polar solvents (by ET_{30}[11]) were more favorably released from the cavity upon binding. The strongest affinity was seen in water, and the lowest in CS_2. Flood has studied the effects of solvent expulsion on halide binding in anion receptors,[12] and Hunter, Ward and Nitschke have investigated solvent effects on guest recognition with metal-ligand capsules and cages.[13] These impressively detailed studies have shown accurate analysis of different factors such as enhanced H-bonding or aromatic stacking for polar guests in different solvents,[13a] or the effects of solvent on the cage fluxionality.[13b]

However, while all these studies are important, they focus on small hosts with defined cavities: there are many hosts (notably metal-ligand complexes) that are capable of catalysis and recognition with much larger cavities and panel gaps. We have previously synthesized Fe_4L_6 cage complexes that display functional groups on their interiors,[14] and applied them as hosts and catalysts. The cages (Figure 1) are formed from either 2,7-dianilino-*9H*-fluorene (cages **F1**-**F3**)[14a,g,i] or 2,7-dianilino-*9H*-carbazole scaffolds (cages **C1**-**C3**).[14h] These hosts are quite unusual, in that they bind neutral organic species strongly (K_a up to 200,000 M^{-1}) in CH_3CN despite their porous structure which allows the substrates to exchange rapidly on the NMR timescale. The catalytic scope is unusual, but can be applied to other systems: several of Nitschke's M-iminopyridine cages show "fast exchange" with small neutral guests,[15a-c] and other cages involving fluorene or carbazole-based ligand cores are known.[15d-i] In addition, the **Fx**/**Cx** cages display internalized functional groups, adding a second layer to the recognition: not only is there a binding pocket, but non-covalent interactions (either attrac-

tive or repulsive) between internal groups and bound guest can affect substrate binding. However, it is not clear *why* the guest binding affinities are so high, and the **Fx/Cx** cages are only soluble in CH_3CN, limiting their applicability as catalysts. Solvent effects are likely a dominant factor, but the lack of broad solubility has limited investigation so far.

The combination of high charge, large size and lipophilic ligands restricts solvent choice: the Ward/Hunter/Nitschke work[13] focused only on CH_3CN and water. The combination of high charge, large size and lipophilic ligands restricts solvent choice, often to either water or acetonitrile (although other polar solvents such as methanol or DMSO are possible). Notably, *M*-iminopyridine cage complexes (the coordination motif in **Fx/Cx**) are invariably soluble in only acetonitrile[1] unless additional factors are exploited to allow dissolution in water.[16] There are cages that dissolve in non-polar solvents,[17] but their binding properties towards neutral guests have not been a focus. Here, we create a series of functionalized Fe_4L_6 cage complexes that are soluble in a broad range of solvents and analyze the effect of solvent and internal function on the molecular recognition properties of neutral substrates.

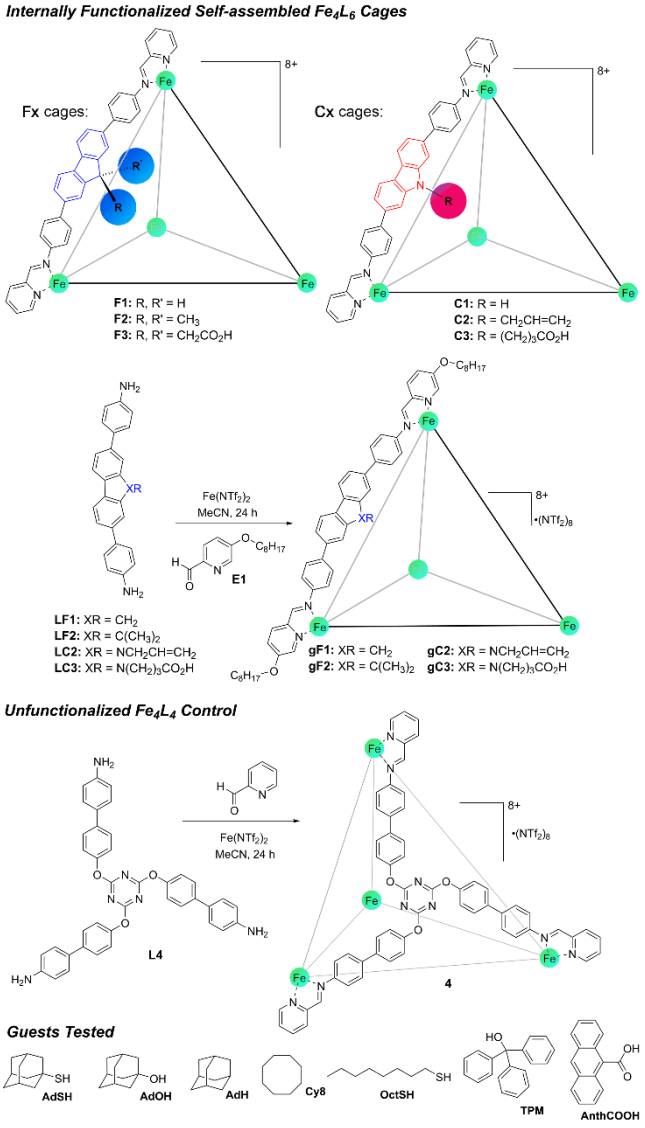

Figure 1. Self-assembled cage complexes tested for molecular recognition properties, and suite of neutral guests (see Supporting Information for synthetic procedures).

RESULTS AND DISCUSSION

While we have measured binding affinities for a series of guests in Fe_4L_6 cages **F1**-**F3**[14a-f,14i] and **C1**[14h] (along with other functionalized variants[14g]) in acetonitrile, this has not been explored systematically or in other solvents. To allow a more detailed study of binding properties, we synthesized a new set of cages with varying internal functions and endgroups. In addition, a similarly sized Fe_4L_4 cage **4** was synthesized for comparison, which has broadly equivalent cavity and portal sizes to **F1**/**C1**, but without internal functions or the polycyclic core.

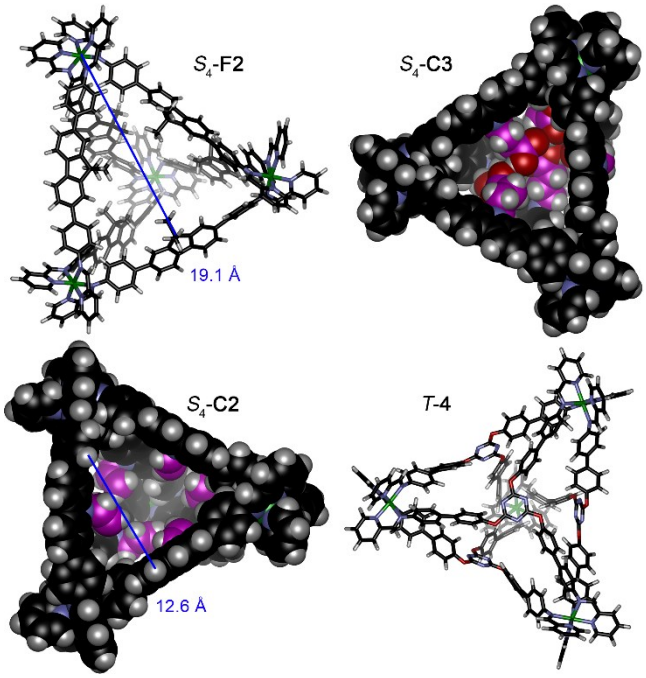

Figure 2. Optimized structures of cages **F2**, **C3**, **C2** (*S*4 isomers) and control cage **4**, illustrating panel gaps and cavity size (semi-empirical, PM7).

As acid-bearing cage **F3**[14a,b,d,f] is quite reactive and sensitive to some additives (as is **C1**), we focused on the more stable cages **F1**, **F2**, **C2**, **C3** and **4**, as well as **gF1**, **gF2**, **gC2** and **gC3**. Ligands **LF1**, **LF2** are known, and the new ligand syntheses of **LC2** and **LC3** followed similar procedures[14a,h] (see Supporting Information): initial derivatization of 2,7-dibromocarbazole by S_N2 reaction with a suitable electrophile (allyl chloride or 4-*tert*-butylbromobutyrate), followed by extension of the ligand via Suzuki coupling with Boc-4-aminophenylboronic acid and deprotection with CF_3CO_3H. Careful neutralization to pH 6.2 after acidic deprotection to form ligand **LC3** was necessary to ensure that the acid group was fully protonated, as carboxylates can interfere with assembly. Control ligand **L4** was synthesized by S_NAr reaction of 4-hydroxy-4'-Boc-aminobiphenyl with trichlorotriazine, followed by acidic deprotection. The lipophilic aldehyde **E1** was synthesized via simple alkylation of 5-hydroxy-2-formylpyridine with base and alkyl iodides. The various cage complexes were assembled using similar procedures: ligand (3 mol.-eq.), aldehyde (6 mol.-eq.) and $Fe(NTf_2)_2$ (2 mol.-eq.) were

combined in dry CH_3CN and refluxed for 24 h (the metal:ligand ratio was 1:1 for the M_4L_4 cage **4**). For ease of discussion, we will refer to the cages with pyridyl endcaps **F1**, **F2**, **C2**, **C3** and **4** as "polarophilic" cages, and the lipidated **gF1**, **gF2**, **gC2** and **gC3** variants as "lipophilic" cages. The isolation procedures for the polarophilic and lipophilic cages were broadly similar: both could be isolated by washing with Et_2O and 20:1 Et_2O:CH_3CN.

The Fe_4L_6 cages all form as mixtures of $T/S_4/C_3$ isomers, and have broadly similar structural characteristics. Optimized structures are shown in Figure 2, which illustrates the structure and the large panel gaps between the ligands, as well as the similarity in size between cages **1**-**3** and **4**. Unfortunately, the large open portals in the structures caused cavity volume calculations in MoloVol[18] to be ineffective, as the cavities are not "enclosed", so portal diameter will be discussed instead. For example, the distance between van der Waals radii of atoms at the periphery of cage **C2** is as much as 12.6 Å (Figure 2), so it is safe to say that guest entry and exit is unrestricted. The cavity of **F2** with internal methyl groups can be filled by approximately 44 molecules of CH_3CN: the larger butyric acid functions in **C3** pinch off the cavity, and only approximately 28 molecules occupy the interior in that case (for optimized structures, see Figure S-186). Obviously, the large entry portals can easily allow rapid solvent exchange, so any definition of cavity "occupation" is only an estimate, but this adequately illustrates the differences in available internal space between the different cages.

As might be expected, adding octyloxy chains to the peripheral pyridyl endcaps does not appreciably change the core structure. An optimized structure of cage **gF2** is shown in Figure 3a, and while the long alkyl chains are flexible, they are oriented away from the cavity, so there should be minimal interaction between entering/exiting guest molecules and the peripheral octyloxy chains. The chains do cause some minor, yet interesting differences in the NMR spectra, though – as can be seen in Figure 3c, the chemical shifts for the imine protons in the **F2** and **gF2** ^{1}H NMR spectra are different, and the $T/S_4/C_3$ isomer ratio is slightly altered.

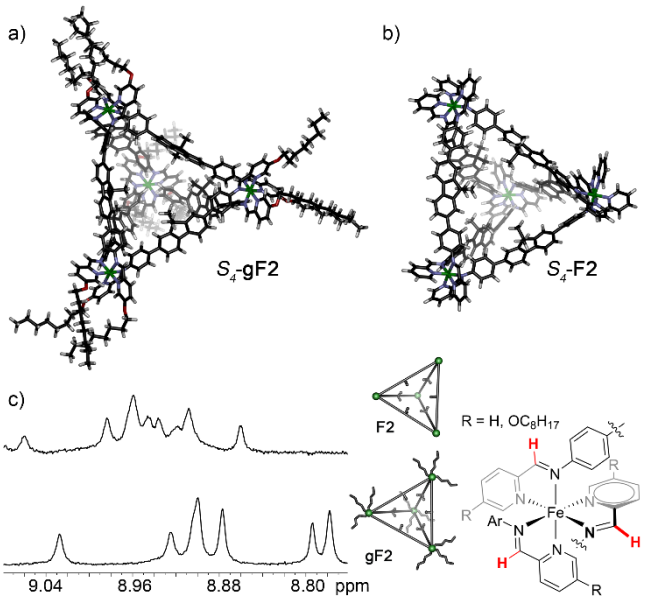

Figure 3. Optimized structures of a) lipophilic cage S_4-**gF2** (semi-empirical, PM7); b) polarophilic cage S_4-**F2** (PM7). c) Expansions of the ^{1}H NMR spectra of **F2** and **gF2** (imine region), showing the different isomer ratios present (CD_3CN, 400 MHz, 298K).

The twelve octyloxy arms on the various **gFx**/**gCx** cages were effective in solubilizing the complexes in more non-polar solvents, but there were limits. Broad solubility tests were performed with the acid-functionalized **gC3**, which was soluble in $CHCl_3$, 1,2-dichloroethane (DCE) and THF. Hydrocarbon solvents (toluene, chlorobenzene, hexanes) were not able to dissolve the cage, nor was dioxane. Among polar solvents, **gC3** was soluble in ethylene glycol, hexafluoroisopropanol (HFIP) and 1,1,1-trifluoroethanol (TFE), but not water, ^{i}PrOH, ^{t}BuOH or allyl alcohol. The chloroform solubility was not consistent across the range of **gFx**/**gCx** cages (**gF2** was insoluble in $CHCl_3$), so we chose a narrowed scope of non-polar solvents to test the molecular recognition – CH_3CN, THF, DCE, ethylene glycol, HFIP, CF_3CH_2OH and varying mixtures of $CHCl_3$/CH_3CN. Comparison tests were performed between the alkylated **gFx**/**gCx** cages and non-alkylated **Fx**/**Cx** cages in CH_3CN, in which all cages were soluble. This broad scope allows a range of variables to be tested to determine the major factors controlling guest binding. Examples are: 1) Packing the interior of the cages obviously changes the available space for guest binding: **F1** is unadorned, **F2** has 12 small lipophilic groups pointed to the interior, **C2** displays six flexible internal allyl groups, and **C3** contains six butyric acid groups, which are larger than the others but can provide (presumably favorable) H-bonding interactions with bound guest. 2) The external octyloxy arms could have an effect on guest binding, even though they do not obviously interact with the cavity. 3) Varying solvent properties will affect guest binding in all cases, a subset of which is 4), the different functions will have different interactions with guests in different solvents, such as putatively stronger H-bonding interactions in non-polar solvents with **gC3**. To interrogate these factors, a broad suite of neutral guest molecules was chosen (Figure 1).[14] These guests included rigid, spherical guests (adamantyl derivatives **AdSH, AdOH, AdH**), aromatic species, either flat (anthroic acid **AnthCOOH**) or polyphenyl (**TPM**), and flexible linear or cyclic guests (octanethiol **OctSH** and cyclooctane **Cy8**). In addition, the guests display a range of coordinating motifs, either weak H-bonding groups (OH, SH), carboxylic acids, or contain no polar groups at all (hydrocarbons).

Binding analysis was performed by titrating the guests into the various hosts in different solvents. As the guest exchange is rapid on the NMR timescale in these hosts, the changes in cage and guest NMR shifts are minimal. This makes NMR titrations too error-prone to be useful (and other possibilities such as diffusion NMR are ESI-MS are not effective), so we focused on UV/Vis spectroscopic titrations. The guests were titrated into solutions of the **Fx/Cx/4** cages (3 μM cage in CH_3CN, 1 μM in all other solvents) and the absorbance changes measured. Examples of the titrations are shown in Figure 4, for all others, see Supporting Information. The binding affinities were calculated using the BindFit software at www.supramolecular.org.[19] In each case, multiple fits were performed using absorbance changes measured at two different frequencies (the exact frequencies depended on the specific cage host and are noted in Figures S-60 – S-185). The isotherms were fit to both 1:1 and non-cooperative 1:2 binding models, and the preferential binding stoichiometry determined by best fit. The full binding affinity data is shown in Tables 1-3 and Figure 4, as well as Supporting Tables S-1 – S-8 and Supporting Figures S-60 – S-185. Tables S-1 – S-8 also show the fitting

results (both successful and failed) for 1:1 and 1:2 binding modes. For clarity, we will break up the discussion into sections, focusing on the effects of changing individual variables.

Effect of Internal Group Variation on Binding Affinity in CH_3CN Solvent

The first test was to determine the effects of varying internal functions on target binding affinity. This focused solely on the polarophilic cages **F1**, **F2**, **C2** and **C3** in CH_3CN using **OctSH, AdOH, AdSH, AnthCOOH** as guests (Table 1). Adding internal functions to the cages does have an effect on guest binding, as expected. The clearest trends are seen between the undecorated fluorene cage **F1** and its dimethyl counterpart **F2**, although there are some notable outliers. Overall, the prevalence of 1:2 binding is lower in the dimethyl cage **F2** than in **F1**: we have previously shown that multiple different guests form 1:2 complexes with **F1**, and some even show positive cooperativity.[14c] Among the guest scope shown here, **OctSH** clearly favors a 1:2 binding mode in **F1**, and good fits for both 1:1 and 1:2 binding are seen with **AnthCOOH**. In contrast, the titration data obtained for these guests and cage **F2** showed poor fits to a 1:2 binding model in all cases (Table S-2). This does not mean that 1:2 binding *cannot* occur, but the 1:1 binding mode appears dominant. This is understandable, as the internal CH_3 groups shrink the available cavity. Other than limiting the formation of heteroternary complexes, there is no obvious conclusion to be drawn between the binding properties of the dimethyl **F2** cage when compared to **F1**. Affinities are generally similar, but **F2** is a better host for some guests (**AdOH**, for example), and a far weaker host for others, notably **OctSH** (Figure 4e, Table 1), which is a strong guest for all other cages (the experiment was repeated multiple times, and the same result obtained, but the explanation is unclear). Overall, slightly shrinking the available cavity size by adding small CH_3 groups to the interior causes small changes in target affinity, as might be expected.

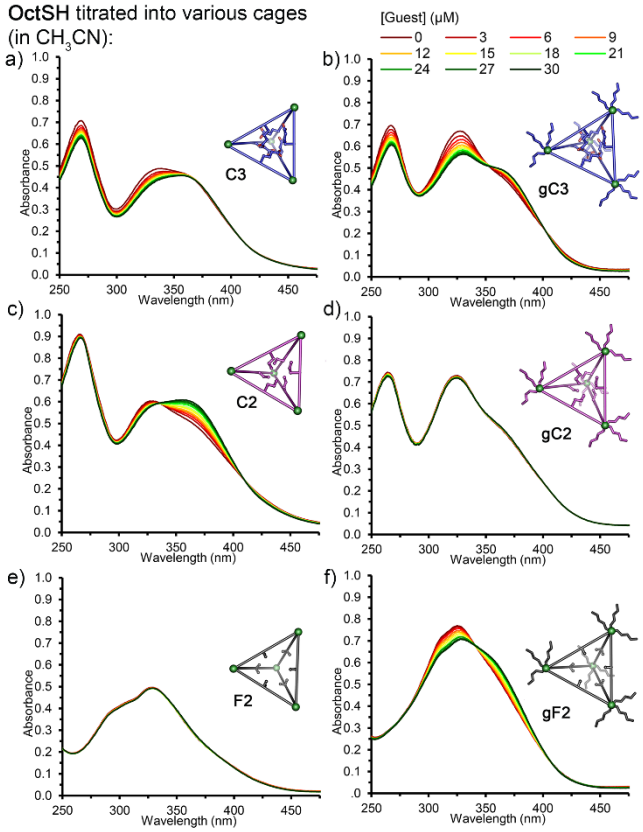

Figure 4. UV/Vis absorbance spectra for the titration of octanethiol (**OctSH**) into 3 μM solutions various cage complexes, CH_3CN, 293 K.

A greater increase in the size of the internal groups causes a clearer trend in affinities. Allyl carbazole cage **C2** binds all four targets in CH_3CN, but does so with a lower affinity than all the other cages: the allyl groups have minimal "positive" interactions with bound guests (such as dipolar interactions or H-bonds), and just block the cavity. This is in contrast with acidic cage **C3**: even though the internalized butyric acid groups are large and should shrink the available cavity, affinities for all the four tested guests (which can all participate in H-bonding, notably) are 3-4 times higher than in the **C2** cage. Again, there is a strong preference for 1:1 binding in these functionalized cages, suggesting that ternary complex formation is more challenging in the packed cages than in the undecorated **F1**.

Affinities were also tested with the similarly sized M_4L_4 cage **4**, but interestingly, no evidence for any guest binding was seen in this case. Even though the Fe-iminopyridine peripheries are the same, and the cavity size and entry/exit portals are broadly similar to **F1**, no observable affinity was seen with guests **OctSH** and **AdOH** in CH_3CN at all (see Figure S-90). Evidently the polycyclic fluorene and carbazole scaffolds (and their internalized groups) are essential for guest recognition – merely creating a cavity does not mean that the cavity will bind substrates. This is actually the "expected" outcome – the small surface area of the ligands, easily rotatable phenyl groups, large cavity and spacious entry portals in **4** are all negative factors when creating a host. It also highlights the unique nature of the **Fx/Cx** scaffold, which has many of those negative elements, but is still a promiscuous host.

Table 1. Binding affinities (K_a, x 10^3 M^{-1}) in functionalized cages: Comparison between polarophilic and lipophilic variants.[a]

Guest (MeCN)	**C3** Cage	**C2** Cage	**F2** Cage	**F1** Cage
OctSH	84.8 ± 4.7	16.3 ± 0.4	N.B.[b]	174 ± 43[c]
AdSH	97.3 ± 7.8	23.6 ± 0.6	51.4 ± 1.9	54.0 ± 3.5
AdOH	130 ± 4.8	26.2 ± 0.7	64.7 ± 4.9	9.6 ± 0.4
Anth-COOH	90.4 ± 8.5	15.0 ± 0.3	20.1 ± 0.5	95.4 ± 5.5[c]
Guest (MeCN)	**gC3** Cage	**gC2** Cage	**gF2** Cage	**gF1** Cage
OctSH	56.2 ± 2.0	N.B.[b]	3.6 ± 0.1	40.5 ± 1.5
AdSH	41.9 ± 2.0[c]	N.B.[b]	12.4 ± 0.4	27.8 ± 1.3
AdOH	43.0 ± 2.5	63.7 ± 2.7	37.7 ± 1.5	80.8 ± 13
Anth-COOH	19.5 ± 1.3	12.7 ± 0.7	7.3 ± 0.2	21.3 ± 0.7

[a] in CH_3CN, [**cage**] = 3 μM, absorbance changes measured at 310/330 nm and 370/380 nm. [b] N.B. = no binding observed. [c] Also shows a propensity for 1:2 affinity, see Table S-2 for full data.

Effect of Octyloxy Chains on Binding Affinity in CH_3CN Solvent

The next task was to determine whether the lipophilic octyloxy chains in the cages had any effect on binding affinity, so the guest affinities were determined in the four lipophilic cages **gF1**, **gF2**, **gC2**, **gC3**, and compared to those in the polarophilic cages **F1**, **F2**, **C2**, **C3**. The guests (**OctSH, AdOH, AdSH, AnthCOOH**) and solvent (CH_3CN) were kept constant, so that the only variable was the pendant arms in the cages. As can be seen in Table 1, guest binding affinity in the lipophilic **gCx/Fx** cages is lower than in the polarophilic **Cx/Fx** cages – for example, **OctSH** affinity drops 35% from **C3** to **gC3**, shows no observable binding in **gC2**, and drops fourfold from **F1** to **gF1**. This trend is generally repeated for the other guests **AdOH**, **AdSH** and **AnthCOOH**, although there are some outliers, indicating (again) that multiple factors are present that control binding. Still, it is interesting that the presence of lipophilic chains at the cage periphery, which appear to have no effect on blocking the cavity, have a deleterious effect on guest binding. Analysis of the absorbance transitions (vide infra) suggests that the guest binding is at the internal fluorene/carbazole ligand sites, but a small amount of competitive association with the external octyloxy chains cannot be ruled out. This would explain the slight lowering in target affinity between the **Fx** and **gFx** cages, although this is speculation, as the low cage solubility and rapid guest exchanges renders NOESY analysis ineffective.

Solvent Effects – Solvents with High Polarity (HFIP, TFE, ethylene glycol)

The nature of solvent polarity is a complex discussion, with numerous metrics that can be used (including dielectric constant, ET_{30}, and more).[12] The complexity of this system makes analysis of the effects of solvent polarity on guest binding challenging. Polar effects such as dipoles and/or hydrogen bonding, London dispersion forces,[7] and the size and shape of the solvent when occupying the cavity of the various cages are all important. Also, these cages do not bind a single solvent molecule, as do smaller hosts,[10] but many, and analysis is restricted to solvents that can dissolve the cages. The **Fx/Cx** cages are restricted to highly polar solvents such as CH_3CN, which shows both high dielectric and polarity (ε = 37.5, ET_{30} = 45.6). The **gFx/gCx** series, on the other hand, allowed a range of solvent polarities to be tested for their effects on guest binding. The two most highly polar solvents (CF_3CH_2OH (TFE, ε = 8.55, ET_{30} = 59.8) and hexafluoroisopropanol (HFIP, ε = 16.7, ET_{30} = 65.3)) completely abrogated any guest binding. As can be seen in Table 2 and Table S-5), no binding affinity is seen in cages **C3**, **gC3** or **gF2** in either TFE or HFIP. This was somewhat surprising, as our assumption had been that Diederich's observation[10] that the more favorable energy gained upon expulsion of more polar solvents from a cavity would drive target affinity in this case, and **OctSH** would be more strongly bound than in the less polar CH_3CN. However, titrations in mixtures of HFIP and CH_3CN also showed no affinity, even when only 10% HFIP was used. Evidently HFIP and TFE are excellent guests for the cage: when HFIP was titrated into cage **gC3** in CH_3CN, a binding affinity of 93.5 ± 7.4 x 10^3 M^{-1} was obtained (Figure S-136). The highly polar HFIP simply outcompetes the neutral guests for the cavity when used as solvent or co-solvent. Interestingly, ethylene glycol (ε = 37.0, ET_{30} = 56.3) was an effective solvent for recognition (see Figures S-138 – S-141 and Table S-6): affinities in cage **C3** ranged from 60 x $10^3 M^{-1}$ (**OctSH**) to 111 x $10^3 M^{-1}$ (**AdSH**), broadly similar to their observed affinities in CH_3CN, although the more polar **AnthCOOH** did not show any affinity in ethylene glycol. Evidently HFIP and TFE are quite unique as solvents: it is not their mere polarity that causes strong cage binding, but a combination of their fluorophilic and H-bonding components. Both HFIP and TFE are "low dielectric, high polarity" solvents, and this mirrors the structure of the added guests: the most successful guests contain relatively large aliphatic/aromatic groups and polar functional groups, and small alcohols like EtOH or ethylene glycol are not bound. Unfortunately, the lipophilic variants **gCx/gFx** were not soluble in ethylene glycol, so we were unable to further test affinities in other highly polar solvents.

Solvent Effects – Weakly Polar Solvents

Tests in highly non-polar solvents such as toluene or chlorobenzene were complicated by the lack of solubility of the cages, even at micromolar concentrations. However, all four lipophilic cages were soluble in both THF (ε = 7.58, ET_{30} = 37.4) and 1,2-dichloroethane (DCE, ε = 10.36, ET_{30} = 41.3, Table 2), so the binding tests were repeated with the same four guests as described previously. Binding in THF was seen for all cages except **gC2**, which was not stable to THF upon dissolution.

Table 2. Binding affinities (K_a, x 10^3 M^{-1}) in functionalized cages in different solvents.[a]

Guest (in THF)	**gC3** Cage	**gC2** Cage	**gF2** Cage	**gF1** Cage
OctSH	19.7 ± 0.7	n.d.[c]	19.3 ± 0.5	10.1 ± 0.1
AdSH	32.7 ± 1.4	n.d.[c]	5.2 ± 0.1	32.0 ± 0.6
AdOH	6.5 ± 0.1	n.d.[c]	7.6 ± 0.2	43.0 ± 1.3
AnthCOOH	12.8 ± 0.4	n.d.[c]	8.1 ± 0.4	17.0 ± 0.5
Guest (in DCE)	**gC3** Cage	**gC2** Cage	**gF2** Cage	**gF1** Cage

OctSH	66.3 ± 7.2	N.B.[b]	87.7 ± 11.0	N.B.[b]
AdSH	52.2 ± 4.2	N.B.[b]	83.6 ± 10.8	17.7 ± 1.7
AdOH	46.2 ± 4.2	N.B.[b]	148 ± 9.5	40.2 ± 6.0
AnthCOOH	7.9 ± 1.6	N.B.[b]	53.0 ± 9.0	26.8 ± 2.8
OctSH in solvent	**C3** Cage	**gC3** Cage	**gF2** Cage	
CF_3CH_2OH	N.B.[b]	N.B.[b]	N.B.[b]	
HFIP	N.B.[b]	N.B.[b]	N.B.[b]	
HFIP:MeCN (1:1)	N.B.[b]	N.B.[b]	N.B.[b]	
HFIP:MeCN (1:9)	N.B.[b]	N.B.[b]	N.B.[b]	

[a] in THF, [**cage**] = 1 μM, absorbance changes measured at 325 nm and 360/370 nm. In DCE, [**cage**] = 1 μM, absorbance changes measured at 280/330 nm and 330/360 nm. In CF_3CH_2OH/HFIP/HFIP:CH_3CN mixtures, [**cage**] = 1 μM, absorbance changes measured at 295 nm and 325 nm. [b] N.B. = no binding observed. [c] cage decomposed in this solvent.

Guest affinities in THF for **gF1** and **gF2** were in the same general range as in CH_3CN: some slight variations were seen for different guests (K_a **OctSH** in cage **gF1** = 40.5 ± 1.5 x 10^3 M^{-1} in CH_3CN vs 10.1 ± 0.1 x 10^3 M^{-1} in THF (i.e. fourfold higher in CH_3CN), whereas K_a **AdSH** in cage **gF1** = 27.8 ± 1.3 x 10^3 M^{-1} in CH_3CN vs 32.0 ± 0.6 x 10^3 M^{-1} in THF, essentially identical). The change in polarity between CH_3CN and THF is large, and this indicates that there is not a linear dependence on solvent polarity that governs the binding affinity in the **Fx/Cx** series of hosts (as was observed by Diederich in his cyclophane case[10]): there are certainly differences in guest binding affinities for different guests in different solvents, but there is no clear trend in affinity that tracks with either dielectric constant or solvent polarity parameters.

1,2-dichloroethane was also tested as a solvent, but introduced a novel challenge: the magnitude of the changes in the titration UV spectra was very small. Isosbestic points were observed in most cases, and the spectra did change upon guest addition, but the errors in fitting were larger in these cases than in the other solvents. The more polar DCE also showed no obvious trend in binding affinities: affinities were higher in the dimethylated fluorene cage **gF2** than the bare **gF1**, and the acidic carbazole cage **gC3** showed strong affinities, whereas no binding was seen with **gC2**.

Solvent Effects – Cavity-based Effects vs Polar Interactions

Table 3. Secondary Effects on Guest Binding.[a]

Guest	Binding affinities (K_a, x 10^3 M^{-1}) in Cage gC3			
	MeCN	MeCN: $CHCl_3$ (1:1)	MeCN: $CHCl_3$ (3:7)	MeCN: $CHCl_3$ (1:9)
OctSH	56.2 ± 2.0	41.4 ± 2.5	46.5 ± 1.5	103 ± 5.4
AdSH	41.9 ± 2.0[c]	86.5 ± 10	36.6 ± 1.8	239 ± 25
AdOH	43.0 ± 2.5	51.3 ± 2.4	60.3 ± 2.0	377 ± 55
AdH	28.4 ± 2.2	17.8 ± 1.6	24.2 ± 1.0	25.5 ± 1.4
Cy8	25.0 ± 3.3	20.1 ± 2.1	33.3 ± 1.0	38.3 ± 0.9
Guest	Binding affinities (K_a, x 10^3 M^{-1}) in Cage gF2			
	MeCN	MeCN: $CHCl_3$ (1:1)	MeCN: $CHCl_3$ (3:7)	MeCN: $CHCl_3$ (1:9)
OctSH	3.6 ± 0.14	53.1 ± 1.4	32.0 ± 1.0	14.7 ± 0.40
AdSH	12.4 ± 0.38	49.7± 1.2	77.1 ± 3.5	48.2 ± 2.4
AdOH	37.7 ± 1.5	42.0 ± 0.76	47.6 ± 2.3	22.6 ± 1.0
AdH	164 ± 21	70.4 ± 3.6	48.0 ± 1.1	37.4 ± 3.1
Cy8	36.5 ± 4.1	69.7 ± 1.4	58.0 ± 1.4	N.B.[b]
Guest	Binding affinities (K_a, x 10^3 M^{-1})			
	gC3 (MeCN)[a]	**gC3** (1:9 MeCN: $CHCl_3$)[b]	**gF2** (MeCN)[b]	**gF2** (1:9 MeCN: $CHCl_3$)[a]
TPM	160 ± 25.6	59.4 ± 2.8	140 ± 15	50.9 ± 4.1

[a] in CH_3CN, [**cage**] = 3 μM, absorbance changes measured at 310/330 nm and 370/380 nm. [b] In CH_3CN:$CHCl_3$ mixtures, [**cage**] = 1 μM, absorbance changes measured at 325 nm and 360/375 nm. [c] Also shows a propensity for 1:2 affinity, see Table S-7 for full data.

The **gF1/gF2/gC2** cages only vary in the amount of accessible cavity space for the guests (and solvents), so they are useful for testing solvent polarity effects on binding: other than some small van der Waals interactions between bound guests and the internal alkyl groups, there are no obvious positive interactions between guest and internal groups of the hosts. This is not the case for **gC3**, which contains internalized acids that can hydrogen-bond with the added guests, a process that should be *more* favorable as solvent polarity is lowered. To further test the effects of the internal acid groups, we narrowed the focus to acid cage **gC3** and dimethylfluorene cage **gF2**, and tested a wider guest range in solvent mixtures of varying polarity, namely combinations of CH_3CN and $CHCl_3$ (Table 3).

These tests illustrated a clear effect of the internal acids on guest binding: as the proportion of $CHCl_3$ increased, the affinity for polar guests in the acid-bearing cage **gC3** markedly increased (Table 3 and Figure 5). For example, K_a **AdSH** in cage **gC3** = 41.9 ± 2.0 x 10^3 M^{-1} in CH_3CN, whereas in 10:90 CH_3CN:$CHCl_3$ K_a = 239 ± 25 x 10^3 M^{-1}. Similar increases in magnitude were seen for the other guests that contained H-bonding groups (**OctSH**, **AdOH**, **AnthCOOH**). The affinity increases were not linearly correlated with solvent ratio, but at high concentrations of $CHCl_3$ in the solvent, the effect was clear. Importantly, this effect did not occur for simple hydrocarbons: when cyclooctane (**Cy8**) or adamantane (**AdH**) were added to cage **gC3**, the affinities were almost completely insensitive to solvent ratio. In addition, when the process was repeated with the non-acid-containing cage **gF2**, the enhancement of guest affinity in the 10:90 CH_3CN:$CHCl_3$ solvent mixture was not seen. This validates the observation seen before, that there is no clear effect of solvent polarity on cavity-based binding for the alkyl- or unfunctionalized cages. However, in the case of the acidic **gC3**, enhanced H-bonding is seen, and the affinity of suitably structured guests is markedly enhanced.

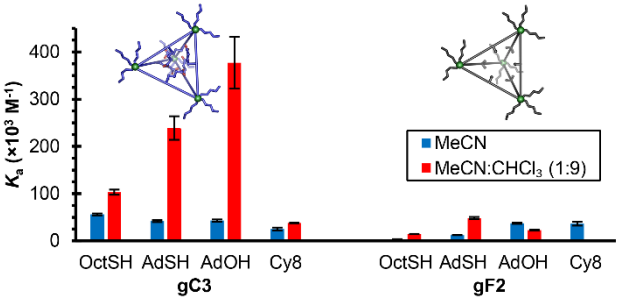

Figure 5. Binding affinity dependence on internal functional groups and solvent. In CH_3CN, [**cage**] = 3 μM, absorbance changes measured at 310/330 nm and 370/380 nm. [b] In CH_3CN:$CHCl_3$ mixtures, [**cage**] = 1 μM, absorbance changes measured at 325 nm and 360/375 nm.

Additional Effects – Large Guests and Bases

Further examples of guest scope were tested in the **gC3** and **gF2** cages, as can be seen in Table 3: the large guest **TPM**, and basic guest imidazole. These two substrates corroborate the importance of two of the binding factors in these cages: the large guest **TPM** is the most strongly bound guest in these two cages, which supports the theory that expulsion of multiple smaller solvent molecules for one large guest is an important driving force. The affinity of **TPM** is lowered in the 1:9 CH_3CN:$CHCl_3$ solvent mix (when compared to CH_3CN alone) for both cages **gC3** and **gF2**. Evidently for large guests, the effects of H-bonding with the internal acids are outweighed by a solvent-based driving force, whereby expulsion of less polar solvents from the cavity is less favorable. The effect of the internal acid groups was also tested by adding imidazole as guest. Unfortunately, studying the effects of strong bases in these cages is problematic, as they can cause decomposition of the cage (for a more detailed discussion of base binding in **F1**, see reference 14i). Both cages **gC3** and **gF2** decomposed in the presence of imidazole or stronger bases, so the H-bonding properties could only be analyzed with weak donors such as alcohols or thiols.

Computational Analysis of Guest Binding Location

One disadvantage with using UV absorption spectroscopy to determine binding affinity in these cases is the lack of positional information, i.e. exactly where the guests are bound in the large cavity. Alternate methods such as scXRD or NMR analysis are either challenging or (in this case) uninformative. However, further investigation of the nature of the UV absorptions and their changes upon guest binding can shed some light on the nature of the recognition. The molecular structures of a single ligand fragment from cages **F1** and **C3** coordinated to two Fe^{2+} atoms at the iminopyridine centers were optimized with density functional theory (DFT) at the PBE0/LANL2DZ level of theory, and the vertical excitation energies and oscillator strengths of the electronic transitions were calculated with time-dependent DFT (TD-DFT) using PBE0 method with both LANL2DZ and def2-TZVP basis sets and the PCM solvent model of acetonitrile, which have been shown to accurately predict UV-vis spectra of ligand-metal systems.[19]

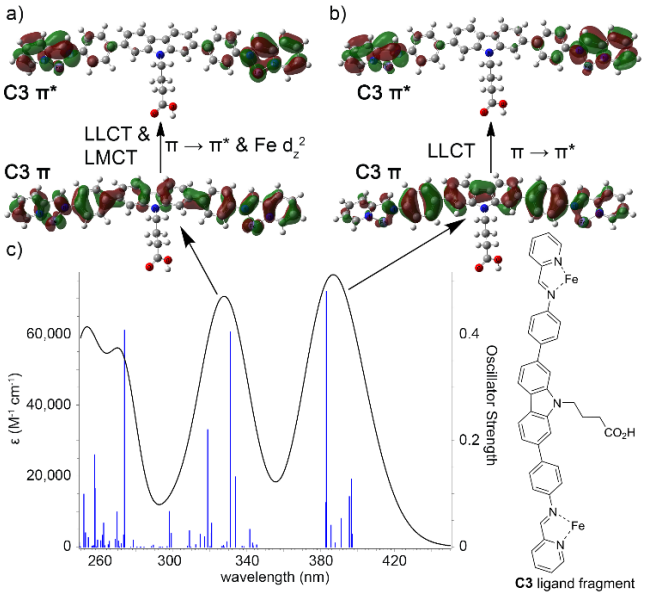

Figure 6. Calculated UV-Vis spectrum of the **C3** cage fragment (PBE0/def2-TZVP) and the molecular orbitals of the two major transitions (PBE0/LANL2DZ).

As can be seen in Figure 6 (and Figures S-190 – S-191), there are two major transitions in the predicted spectrum of the **C3** fragment, which are also seen in the absorption spectrum of **F1**. The predicted transition ~380 nm has a strong oscillator strength of 0.48 at the PBE0/def2-TZVP level of theory. Natural transition orbital (NTO) analysis (PBE0/LANL2DZ) shows this transition is a ligand-to-ligand charge transfer (LLCT) excitation from π orbital located in middle of the ligand to π* molecular orbital on two ends of the ligand. The transition at ~325 nm is a mixture of ligand-to-metal charge transfer (LMCT) and LLCT excitation from π orbital on the ligand to d_z^2 orbital of Fe^{2+} and π* on two ends of the ligand. These two major transitions are also seen for the **F1** fragment (see Figure S-187 – S-188), suggesting that the UV absorption behavior for the fluorene and carbazole ligand scaffolds is similar. These predicted transitions also shed light on where the guest binding interactions occur. In all cases, guest addition leads to a lowering of the cage absorption at ~325 nm (exact number depends on cage), and an increase in cage absorption at ~380 nm (see Figure 2 and Supporting Information). Both of these transitions are *ligand*-centered, suggesting that guest interactions with the central carbazole or fluorene core are important for the recognition. This also explains the "secondary" effects seen with acidic cage **gC3** – interactions between guest and the polycyclic ligand wall bring any H-bonding groups into close proximity with the internal acids. Finally, this data helps explain the lack of binding in control cage **4**: that cage, while superficially similar in overall size and entry portal diameter to the **Fx/Cx** system, lacks the polycyclic walls that are integral to guest binding.

CONCLUSIONS

In summary, we have synthesized a new series of functionalized cage complexes, exploiting lipophilic groups at the pyridyl termini to confer solubility in a range of solvents, and studied the effects of solvent and internal functionality on the molecular recognition properties of the cages. Adding lipophilic chains to the cage exterior confers

solubility in non-polar solvents with minimal interference in the cavity-based recognition process. The presence of polycyclic ring systems in the ligand is essential for the recognition, and optical analysis suggests that the guests have interactions with these walls, causing changes in absorption peaks for ligand-centered transitions.

This experimental and theoretical data allows some conclusions to be drawn about the complex molecular recognition properties of the functionalized **Fx/Cx** cage system, and these conclusions are applicable to other spacious catalytically active metal-ligand cage complexes. The **Fx/Cx** cages are promiscuous hosts, binding neutral organic species of multiple different sizes and shapes in multiple stoichiometries, often with micromolar or submicromolar affinities. Guests with polar or H-bonding groups are generally bound more strongly than simple hydrocarbons, and packing the interior of the cage lowers guest affinity. However, incorporating acidic or H-bonding groups on the cage interior adds a second layer of driving force for polar guest recognition, which can overcome loss of affinity due to increased cavity packing.

Whereas other, simpler macrocyclic systems show guest binding affinity linearly related with solvent polarity[10] due to the increased favorability of more polar solvents self-associating upon expulsion from the cavity, the molecular recognition properties of the **Fx/Cx** cage scaffold are more nuanced. The large cavities can be occupied by multiple solvent molecules (as many as 44), so while guest binding is partly driven by entropically favorable expulsion of multiple small solvent molecules upon binding a larger guest, the solvents do not experience a large change in environment between bound and free states: most of the bound CH_3CN molecules are surrounded by other CH_3CN molecules in the cavity, so a simple linear model is not applicable here. Certain solvents have very clear effects: solvents with both H-bonding and lipophilic sites such as HFIP and TFE are excellent guests for the host cavities and eliminate all guest binding. Other highly polar solvents such as ethylene glycol are similar to CH_3CN, and allow high affinities for neutral guests.

Lower polarity solvents often confer lower affinities in unfunctionalized cages. Importantly, the nature of the solvent has greatest effect on the molecular recognition properties of the catalytically active acidic cage **gC3**. In this case, the presence of the internal acid group allows favorable H-bonding or ion bridge interactions with H-bonding guests or bases, and this factor is enhanced in less polar solvents (such as mixtures of $CHCl_3$ and CH_3CN). This effect is not seen for hosts and guests which do not contain polar groups (cage **gF2** of guest **AdH**, for example), and guest affinity is strongly reduced when large non-polar groups are internalized in the host cavity (e.g. cage **C2**). This suggests that non-polar solvents will be an effective medium for **gC3**-catalyzed reactions, an area we are currently investigating. Balancing directed host:guest interactions (e.g. H-bonds) with entropic effects from solvent displacement is essential for planning supramolecular catalysis with functionalized cages in non-polar solvents.

EXPERIMENTAL

General Information. Cages **F1** and **F2** were synthesized according to literature procedures (see those publications for full characterization data).[14a,i] ^1H , ^{13}C and 2D NMR spectra were recorded on Bruker Avance NEO 400 MHz or Bruker Avance 600 MHz NMR spectrometers, which were automatically tuned and matched to the correct operating frequencies. Structural assignments were made with additional information from gCOSY, gHSQC, and gDOSY experiments. Proton (^1H) and carbon (^{13}C) chemical shifts are reported in parts per million (δ) with respect to tetramethylsilane (TMS, δ=0), and referenced internally with respect to the protio solvent impurity for CD_3CN (^1H: 1.94 ppm, ^{13}C: 118.3 ppm), $CDCl_3$ (^1H: 7.26 ppm, ^{13}C: 77.2 ppm), or DMSO-d_6 (^1H: 2.50 ppm, ^{13}C: 39.5 ppm). Deuterated NMR solvents were obtained from Cambridge Isotope Laboratories, Inc., Andover, MA, and used without further purification. Spectra were digitally processed (phase and baseline corrections, integration, peak analysis) using Bruker Topspin 1.3 and MestreNova. All chemicals were obtained from Aldrich Chemical Company (St. Louis, MO), Combi-Blocks (San Diego, CA) or Fisher Scientific (Fairlawn, NJ), and were used as received. Solvents were dried through a commercial solvent purification system (Pure Process Technologies, Inc.). UV/Vis spectroscopy was performed on a Cary 60 Photospectrometer using the Varian Scans program to collect data. The mass spectrometric samples of cages **C3**, **gC3**, **C2**, **gC2**, **gF2**, **gF1**, and **4** were prepared in 100% MeCN and infused into an Orbitrap Velos Pro mass spectrometer (Thermo Fisher Scientific, San Jose, CA, USA) with a homebuilt nanoESI source. The spray voltage, capillary temperature, and the S-lens RF level were set to 1.7 kV, 160 °C, and 45% respectively. Full mass spectra were acquired with a resolution of r = 30 000. Thermo Xcalibur was used to analyze MS data and prepare the predicted isotope patterns. For all other molecules, high resolution accurate mass spectral data were obtained from the Analytical Chemistry Instrumentation Facility at the University of California, Riverside, on an Agilent 6545 QTOF LC/MS instrument. Melting points were obtained with a Mel-Temp melting point apparatus.

General Procedure for Cage Synthesis. Deprotected ligand (e.g. **LF1**, 1 equiv, 0.08 mmol) was added to a Schlenk flask with $Fe(NTf_2)_2$ (30 mg, 0.7 eq, 0.05 mmol), 8 mL dry MeCN, and either 2-pyridinecarboxaldehyde (14.4 μL, 2 equiv, 0.16 mmol) or 5-(octyloxy)-2-pyridinecarboxaldehyde (37 mg, 2 equiv, 0.16 mmol). After stirring 16 h at 80 °C, the reaction mixture was cooled to room temperature and any solids removed *via* vacuum filtration. The remaining acetonitrile was removed *in vacuo* and the solid residue briefly sonicated in Et_2O. This was followed by filtration of the solid, which was washed with Et_2O (20 mL) and 20:1 Et_2O:MeCN (50 mL) and collected. For full synthetic schemes, procedures and characterization of cage complexes and precursor ligands, see Supporting Information.

General Procedure for Binding Affinity Calculations. A 3.0 μM solution of cage was prepared in 3 mL spectroscopic grade MeCN, or a 1.0 μM solution in all other solvents, via dilutions from a 0.3 mM stock solution, and added to a UV-Vis cuvette. To this solution was then added 1 μL aliquots from a 9.0 mM solution of the corresponding guest molecule, equating to one molar equivalent guest to cage in MeCN solutions or three molar equivalents in all other solvents. These additions were continued until there was no observable change in the absorption spectrum. Binding affinities were calculated using BindFit at supramolecular.org[18] *via* linear regression analysis using the Nelder-Mead method from the change in absorbance at two points, typically between 300-330 nm and 360-390 nm.

Computational Methods. The molecular structures of cage **F1** (Figure 2) and ligand fragments **F1**, **C3** (Figure 5) were optimized with density functional theory (DFT) at the B3LYP/LANL2DZ and

PBE0/LANL2DZ level of theory, respectively. All other cage structures, notably those with >450 atoms (e.g. lipophilic cage **F2**, **C2**, **C3** and **gF2**, Figure 3) were optimized with the semi-empirical method PM7. The vertical excitation energies and oscillator strengths of the electronic transitions were calculated with TD-DFT using PBE0 method with both LANL2DZ and def2-TZVP basis sets, which are believed to have balanced performance for predicting UV-vis spectra of ligand-metal systems with relatively good accuracy and computational efficiency.[20] To obtain a straightforward chemical orbital interpretation of the excitations, the major transitions with strong oscillator strengths were further analyzed with NTO methods at the PBE0/LANL2DZ level of theory.[21] The polarizable continuum model with the integral equation formalism variant (IEFPCM) as the implicit solvent model was employed to account for the dielectric environment of acetonitrile solvent within affordable computational cost.[22] The UV-vis spectra calculated in this work were all plotted with a peak half-width of 0.15 eV. All the DFT calculations performed in this work were accomplished with Gaussian 16 and visualized with GaussView software, while the semi-empirical method PM7 was used to optimize large molecules utilizing MOPAC package with the COSMO solvent model.[23]

ASSOCIATED CONTENT

Data Availability Statement

The data underlying this study are available in the published article and its Supporting Information.

Supporting Information

Supporting Information (pdf): Synthesis and characterization of new compounds, binding analysis including spectroscopic data and binding isotherms, and computational analysis of cage structures and optical transitions. Supporting Information (Excel): Cartesian Coordinates for calculated structures. This material is available free of charge via the Internet at http://pubs.acs.org.

AUTHOR INFORMATION

Corresponding Authors

* E-mail: richard.hooley@ucr.edu

ACKNOWLEDGMENTS

The authors would like to thank the National Science Foundation (CHE-2303142 to R. J. H. and CHE-2155232 to J. Z.) and the National Institutes of Health (1R01AG066626 to R. R. J.) for funding.

REFERENCES

(1) McTernan, C. T.; Davies, J. A.; Nitschke, J. R. Beyond platonic: how to build metal–organic polyhedra capable of binding low-symmetry, information-rich molecular cargoes. *Chem. Rev.* **2022**, *122*, 10393–10437.

(2) Beatty, M. A.; Hof, F. Host–guest binding in water, salty water, and biofluids: general lessons for synthetic, bio-targeted molecular recognition. *Chem. Soc. Rev.* **2021**, *50*, 4812–4832.

(3) (a) Langton, M. J.; Serpell, C. J.; Beer, P. D. Anion recognition in water: recent advances from a supramolecular and macromolecular perspective. *Angew. Chem. Int. Ed.* **2016**, *55*, 1974–1987. (b) Evans, N. H.; Beer, P. D. Advances in anion supramolecular chemistry: from recognition to chemical applications. *Angew. Chem. Int. Ed.* **2014**, *53*, 11716–11754. (c) Custelcean, R. Anion Encapsulation and Dynamics in Self-Assembled Coordination Cages. *Chem. Soc. Rev.* 2014, *43*, 1813–1824.

(4) (a) Laughrey, Z.; C. Gibb, B. Water-soluble, self-assembling container molecules: an update. *Chem. Soc. Rev.* **2011**, *40*, 363–386. (b) Jordan, J. H.; Gibb, B. C. Molecular containers assembled through the hydrophobic effect. *Chem. Soc. Rev.* **2014**, *44*, 547–585.

(5) (a) Escobar, L.; Ballester, P. Molecular recognition in water using macrocyclic synthetic receptors. *Chem. Rev.* **2021**, *121*, 2445–2514. (b) Kubik, S. When molecules meet in water-recent contributions of supramolecular chemistry to the understanding of molecular recognition processes in water. *ChemistryOpen* **2022**, *11*, e202200028.

(6) (a) Rizzuto, F. J.; von Krbek, L. K. S.; Nitschke, J. R. Strategies for binding multiple guests in metal-organic cages. *Nat. Rev. Chem.* **2019**, *3*, 204–222. (b) Fujita, M.; Umemoto, K.; Yoshizawa, M.; Fujita, N.; Kusukawa, T.; Biradha, K. Molecular paneling *via* coordination. *Chem. Commun.* **2001**, 509–518. (c) Brown, C. J.; Toste, F. D.; Bergman, R. G.; Raymond, K. N. Supramolecular catalysis in metal-ligand cluster hosts. *Chem. Rev.* **2015**, *115*, 3012–3035. (d) Davis, A. V.; Raymond, K. N. The Big Squeeze: Guest Exchange in an M_4L_6 Supramolecular Host. *J. Am. Chem. Soc.* **2005**, *127*, 7912–7919.

(7) (a) Schneider, H.-J. Binding Mechanisms in Supramolecular Complexes. *Angew. Chem. Int. Ed.* **2009**, *48*, 3924 – 3977. (b) Hof, F.; Craig, S. L.; Nuckolls, C.; Rebek, J., Jr. Molecular encapsulation. *Angew. Chem. Int. Ed.* **2002**, *41*, 1488–1508.

(8) (a) Blackburn, M. A. S.; Wagen, C. C.; Bodrogean, M. R.; Tadross, P. M.; Bendelsmith, A. J.; Kutateladze, D. A.; Jacobsen, E. N. Dual-Hydrogen-Bond Donor and Brønsted Acid Cocatalysis Enables Highly Enantioselective Protio-Semipinacol Rearrangement Reactions. *J. Am. Chem. Soc.* **2023**, *145*, 15036–15042. (b) Q. Zhang, L. Catti, K. Tiefenbacher, Catalysis inside the Hexameric Resorcinarene Capsule. *Acc. Chem. Res.* **2018**, *51*, 2107–2114.

(9) (a) Mugridge, J. S.; Zahl, A.; van Eldik, R.; Bergman, R. G.; Raymond, K. N. Solvent and Pressure Effects on the Motions of Encapsulated Guests: Tuning the Flexibility of a Supramolecular Host. *J. Am. Chem. Soc.* **2013**, *135*, 4299–4306. (b) Ryan, H. P.; Fishman, Z. S.; Pawlik, J. T.; Grommet, A.; Musial, M.; Rizzuto, F.; Booth, J. C.; Long, C. J.; Schwarz, K.; Orloff, N. D. Nitschke, J. R. Stelson, A. C. Quantifying the Effect of Guest Binding on Host Environment. *J. Am. Chem. Soc.* **2023**, *145*, 19533–19541. (c) Kang, J. M.; Rebek, J., Jr. Entropically driven binding in a self-assembling molecular capsule. *Nature.* **1996**, *382*, 239–241.

(10) Smithrud, D. B.; Sanford, E. M.; Chao, I.; Ferguson, S. B.; Carcanague, D. R.; Evanseck, J. D.; Houk, K. N.; Diederich, F. Solvent effects in molecular recognition. *Pure Appl. Chem.* **1990**, *62*, 2227–2236. (b) Ferguson, S. B.; Sanford, E. M.; Seward, E. M.; Diederich, F. Cyclophane-Arene Inclusion Complexation in Protic Solvents: Solvent Effects versus Electron Donor-Acceptor Interactions. *J. Am. Chem. Soc.* **1991**, *113*, 5410–5419.

(11) Reichardt, C. Solvatochromic Dyes as Solvent Polarity Indicators. *Chem. Rev.* **1994**, *94*, 2319–2358.

(12) Liu, Y.; Sengupta, A.; Raghavachari, K.; Flood, A. H. Anion binding in solution: beyond the electrostatic regime. *Chem* **2017**, 3, 411–427.

(13) (a) Whitehead, M.; Turega, S.; Stephenson, A.; A. Hunter, C.; D. Ward, M. Quantification of solvent effects on molecular recognition in polyhedral coordination cage hosts. *Chem. Sci.* **2013**, *4*, 2744–2751. (b) Bolliger, J. L.; Ronson, T. K.; Ogawa, M.; Nitschke, J. R. Solvent effects upon guest binding and dynamics of a $Fe^{II}_4L_4$ cage. *J. Am. Chem. Soc.* **2014**, *136*, 14545–14553.

(14) (a) Holloway, L. R.; Bogie, P. M.; Lyon, Y.; Ngai, C.; Miller, T. F.; Julian, R.R.; Hooley, R.J. Tandem reactivity of a self-assembled cage catalyst with endohedral acid groups. *J. Am. Chem. Soc.* **2018**, *140*, 8078–8081. (b) Bogie, P. M.; Holloway, L. R.; Ngai, C.; Miller, T. F.; Grewal, D. K.; Hooley, R. J. A self-assembled cage with endohedral acid groups both catalyzes substitution reactions and controls their molecularity. *Chem. Eur. J.* **2019**, *25*, 10232. (c) Ngai, C.; Bogie, P. M.; Holloway, L. R.; Dietz, P. C.; Mueller, L. J.; Hooley, R. J. Cofactor-mediated nucleophilic substitution catalyzed by a self-assembled holoenzyme mimic. *J. Org. Chem.* **2019**, *84*, 12000–12008. (d) Ngai, C.; Sanchez-Marsetti, C. M.; Harman, W. H.; Hooley, R. J. Supramolecular catalysis of the oxa-Pictet–Spengler reaction with an endohedrally functionalized self-assembled cage complex. *Angew. Chem. Int. Ed.* **2020**, *59*, 23505–23509. (e) da Camara, B.; Dietz, P. C.; Chalek, K. R.; Mueller, L. J.; Hooley, R. J. Selective, cofactor-mediated catalytic oxidation of alkanethiols in a self-assembled cage host. *Chem. Commun.* **2020**, *56*,

14263–14266. (f) Ngai, C.; da Camara, B.; Woods, C. Z.; Hooley, R. J. Size- and shape-selective catalysis with a functionalized self-assembled cage host. *J. Org. Chem.* **2021**, *86*, 12862–12871. (g) Ngai, C.; Wu, H.-T.; da Camara, B.; Williams, C. G.; Mueller, L. J.; Julian, R. R.; Hooley, R. J. Moderated basicity of endohedral amine groups in an octa-cationic self-assembled cage. *Angew. Chem. Int. Ed.* **2022**, *61*, e202117011. (h) Woods, C. Z.; Wu, H.-T.; Ngai, C.; da Camara, B.; Julian, R. R.; Hooley, R. J. Modifying the internal substituents of self-assembled cages controls their molecular recognition and optical properties. *Dalton Trans.* **2022**, *51*, 10920–10929. (i) da Camara, B.; Woods, C. Z.; Sharma, K.; Wu, H.-T.; Farooqi, N. S.; Chen, C.; Julian, R. R.; Vander Griend, D. A.; Hooley, R. J. Catalytic inhibition of base-mediated reactivity by a self-assembled metal-ligand host. *Chem. Eur. J.* **2023**, *29*, e202302499.

(15) (a) Rizzuto, F. J.; Carpenter, J. P.; Nitschke, J. R. Multisite binding of drugs and natural products in an entropically favorable, heteroleptic receptor. *J. Am. Chem. Soc.* **2019**, *141*, 9087–9095. (b) Meng, W.; Breiner, B.; Rissanen, K.; Thoburn, J. D.; Clegg, J. K.; Nitschke, J. R. A self-assembled M_8L_6 cubic cage that selectively encapsulates large aromatic guests. *Angew. Chem., Int. Ed.* **2011**, *50*, 3479–3483. (c) Ramsay, W. J.; Szczypiński, F. T.; Weissman, H.; Ronson, T. K.; Smulders, M. M. J.; Rybtchinski, B.; Nitschke, J. R. Designed enclosure enables guest binding within the 4200 $Å^3$ cavity of a self-assembled cube. *Angew. Chem., Int. Ed.* **2015**, *54*, 5636–5640. (d) A. Rowland, C.; R. Lorzing, G.; Bhattacharjee, R.; Caratzoulas, S.; A. Yap, G. P.; D. Bloch, E. Design and Synthesis of Aryl-Functionalized Carbazole-Based Porous Coordination Cages. *Chem. Comm.* **2020**, *56*, 9352–9355. (e) Zhou, W.; Sarma, T.; Su, Y.; Lei, C.; Sessler, J. L. Kinetic Trapping of a Cobalt(II) Metallocage Using a Carbazole-Containing Expanded Carbaporphyrinoid Ligand. *Chem. Sci.* **2022**, *13*, 692–697. (f) Zhang, B.; Lee, H.; Holstein, J. J.; Clever, G. H. Shape-Complementary Multicomponent Assembly of Low-Symmetry Co(III)Salphen-Based Coordination Cages. *Angew. Chem. Int. Ed.* **2024**, *63*, e202404682. (g) Platzek, A.; Juber, S.; Yurtseven, C.; Hasegawa, S.; Schneider, L.; Drechsler, C.; Ebbert, K. E.; Rudolf, R.; Yan, Q.-Q.; Holstein, J. J.; Schäfer, L. V.; Clever, G. H. Endohedrally Functionalized Heteroleptic Coordination Cages for Phosphate Ester Binding. *Angew. Chem. Int. Ed.* **2022**, *61*, e202209305. (h) Zhang, H.-N.; Lin, Y.-J.; Jin, G.-X. Selective Construction of Very Large Stacking-Interaction-Induced Molecular 8_{18} Metalla-Knots and Borromean Ring Using Curved Dipyridyl Ligands. *J. Am. Chem. Soc.* **2021**, *143*, 1119–1125. (i) Shi, J.; Xu, W.; Yu, H.; Wang, X.; Jin, F.; Zhang, Q.; Zhang, H.; Peng, Q.; Abdurahman, A.; Wang, M. A Highly Luminescent Metallo-Supramolecular Radical Cage. *J. Am. Chem. Soc.* **2023**, *145*, 24081–24088.

(16) (a) Mal, P.; Schultz, D.; Beyeh, K.; Rissanen, K.; Nitschke, J. R. An unlockable-relockable iron cage by subcomponent self-assembly. *Angew. Chem. Int. Ed.* **2008**, *47*, 8297–8301. (b) Bolliger, J. L.; Belenguer, A. M.; Nitschke, J. R. Enantiopure Water-Soluble $[Fe_4L_6]$ Cages: Host–Guest Chemistry and Catalytic Activity. *Angew. Chem. Int. Ed.* **2013**, *52*, 7958–7962.

(17) (a) Percástegui, E. G.; Mosquera, J.; Nitschke, J. R. Anion Exchange Renders Hydrophobic Capsules and Cargoes Water-Soluble. *Angew. Chem. Int. Ed.* **2017**, *56*, 9136–9140. (b) Grommet, A. B.; Hoffman, J. B.; Percástegui, E. G.; Mosquera, J.; Howe, D. J.; Bolliger, J. L.; Nitschke, J. R. Anion Exchange Drives Reversible Phase Transfer of Coordination Cages and Their Cargoes. *J. Am. Chem. Soc.* **2018**, *140*, 14770– 14776. (c) Zhang, D.; Ronson, T. K.; Lavendomme, R.; Nitschke, J. R. Selective Separation of Polyaromatic Hydrocarbons by Phase Transfer of Coordination Cages. *J. Am. Chem. Soc.* **2019**, *141*, 18949–18953.

(18) (a) www.molovol.com; (b) Maglic, J.B.; Lavendomme, R. MoloVol: an easy-to-use program for analyzing cavities, volumes and surface areas of chemical structures. *J. Appl. Cryst.* **2022**, *55*, 1033–1044.

(19) (a) Hibbert, D. B.; Thordarson, P. The death of the Job plot, transparency, open science and online tools, uncertainty estimation methods and other developments in supramolecular chemistry data analysis. *Chem. Commun.* **2016**, *52*, 12792–12805. (b) Thordarson, P. Determining association constants from titration experiments in supramolecular chemistry. *Chem. Soc. Rev.* **2011**, *40*, 1305–1323.

(20) (a) Adamo, C.; Barone, V. Toward reliable density functional methods without adjustable parameters: the PBE0 model. *J. Chem. Phys.* **1999**, *110*, 6158–6170. (b) Adamo, C.; Barone, V. Inexpensive and accurate predictions of optical excitations in transition-metal complexes: the TDDFT/PBE0 route. *Theor. Chem. Acc.* **2000**, *105*, 169–172. (c) Adamo, C.; Jacquemin, D. The calculations of excited-state properties with time-dependent density functional theory. *Chem. Soc. Rev.* **2013**, *42*, 845–856. (d) Latouche, C.; Skouteris, D.; Palazzetti, F.; Barone, V. TD-DFT benchmark on inorganic Pt(II) and Ir(III) complexes. *J. Chem. Theory Comput.* **2015**, *11*, 3281–3289.

(21) Martin, R. L. Natural transition orbitals. *J. Chem. Phys.* **2003**, *118*, 4775–4777.

(22) Tomasi, J.; Mennucci, B.; Cammi, R. Quantum mechanical continuum solvation models. *Chem. Rev.* **2005**, *105*, 2999–3094.

(23) Stewart, J. J. P. Optimization of parameters for semiempirical methods VI: more modifications to the NDDO approximations and re-optimization of parameters. *J. Mol. Model.* **2013**, *19*, 1–32.

TOC Graphic: